Journal of Materials Science and Chemical Engineering, 2026, 14(9), 1-13
https://www.scirp.org/journal/msce
ISSN Online: 2327-6053
ISSN Print: 2327-6045

Spectroscopic and Electrochemical Studies on Photoactive Thin Films of Poly (2,5-Di(2-thienyl)-1H-pyrrole) (PSNS) in Gel Electrolytes: Influence of the Pyrrole NH Group

Kasem K. Kasem*, Hisako Masuda, Christian Chauret, Cullen Reilly O'Marrah, Hannah Victoria Hermansen

School of Sciences, Indiana University Kokomo, Kokomo, USA
Email: *kkasem@iu.edu

How to cite this paper: Kasem, K.K., Masuda, H., Chauret, C., O'Marrah, C.R. and Hermansen, H.V. (2026) Spectroscopic and Electrochemical Studies on Photoactive Thin Films of Poly (2,5-Di(2-thienyl)-1H-pyrrole) (PSNS) in Gel Electrolytes: Influence of the Pyrrole NH Group. *Journal of Materials Science and Chemical Engineering*, **14**, 1-13.
https://doi.org/10.4236/msce.2026.149001

Received: July 23, 2026
Accepted: September 7, 2026
Published: September 10, 2026

Abstract

Photo-electrochemical (PEC) and spectroscopic studies were conducted on poly (2,5-di(2-thienyl)-1H-pyrrole) (PSNS) in a gel electrolyte. The results were compared with those of 2,2'-bithiophene (PBTh). The results show that incorporating a pyrrole ring into a pure thiophene monomer produces a polymer that shows no hole accumulation and exhibits random electron-hole pair production in its PEC. Absorption spectra indicate that PSNS has a band gap that ranges from 2.3 to 3.1 eV, whereas DFT calculations show that pure PSNS has an approximate band gap of 2.0 eV. Furthermore, EIS studies reveal that PSNS exhibits lower real impedance than PBTh. This can be correlated to several factors such as porosity, doping, and the morphology of each polymer. Both studied polymers were electrochromic and exhibited fluorescence emission. The gel electrolyte demonstrates sustainable functionality, evidenced by the reproducible photo-electrochemical results.

Keywords

Optical, Electrochemistry, Organic Semiconductors, Gel Electrolytes, Photocurrent

1. Introduction

The increasing demand for organic semiconductors demands the development of new organic materials that can effectively form desirable heterojunctions. The functionality of these heterojunctions relies on distinct charge-carrier distribu-

tions, which can be classified into electron- and hole-accumulation and depletion layers [1]. Many organic polymer semiconductors are inherently p-type due to their low electron affinity, which results from a shallow lower unoccupied molecular orbital (LUMO) [2]. This property of p-type organic semiconductors makes them particularly valuable in the design of efficient optoelectronic devices, highlighting the importance of the hole-accumulation layer. This interfacial layer plays a crucial role in reducing the charge-injection barrier at the electrode/active layer interface, thereby promoting efficient charge extraction and enhancing overall device performance [3]-[6].

Polythiophenes possess enhanced planarity, extended π-conjugation, and ordered packing, which together enable more effective charge delocalization. This results in a higher capacity for hole accumulation when subjected to doping or photoexcitation. For monomers containing S and N as heteroatoms, such as thienyl pyrrole (SN), the non-planar backbone of poly SN leads to less efficient charge delocalization and increased localized hole trapping. This leads to a reduced density of mobile charge carriers and decreased hole accumulation efficiency. Several studies were conducted on the synthesis and electrochemical properties of S-based heterocyclic compounds, to name a few [7]-[11].

Polymers of heterocyclic monomers have been synthesized using an electrochemical technique [12]. Several studies have been conducted on thiophene polymers combined with pyrrole (Poly SN) [13], and those combined with oxygen, such as poly-thiofuran (PSO) [14], to investigate how the structure of the monomers affects the optical and electrical properties of the resulting photoactive polymer.

Sulfur-containing heterocyclic compounds, such as thiophenes and their derivatives, are crucial in designing photoactive polymers. The addition of sulfur atoms can significantly change the electronic and optical properties of these materials. The structure of the sulfur heterocycle and the polymer backbone allows for tuning of properties such as refractive index, light absorption, and emission wavelengths. Some poly(thioether) materials exhibit strong luminescence when polymer chains cluster, a phenomenon triggered by specific conditions.

In this study, we posit that incorporation of pyrrole NH into the monomer structure may affect the optical/electrochemical properties of PSNS (poly 2,5-di(2-thienyl)-1H-pyrrole) compared to PBTh (poly bithiophene) in gel electrolytes.

Our choice of gel electrolytes arises from their merger of the high ionic conductivity of liquids with the structural stability of solids. This combination eliminates the risks associated with free-flowing fluids, enhancing safety against leaks and fires. Gel electrolytes also offer excellent flexibility for wearable electronics, reduce the formation of harmful dendrites, and enhance the overall cycle life and thermal durability of advanced energy storage systems. Gel electrolytes that contain I^-/I_3^- exhibit a redox potential suitable for the potential window of studies. The goal was to determine if incorporating a pyrrole ring into pure thiophene-based monomers significantly changed the PEC behavior outcomes of PSNS in gel electrolytes.

2. Experimental

2.1. Reagents

The monomers 2,5-di(2-thienyl)-1H-pyrrole, 2.2' bithiophene, and lithium perchlorate ($LiClO_4$), and polyethylene glycol (PEG) were, unless otherwise stated of analytical grade.

2.2. Preparations

FTO (fluorine-doped tin oxide)/organic interface assemblies FTO/PSNS, and FTO/PBTh (poly 2.2' bithiophene) thin films were prepared using oxidative electrochemical techniques as previously described [15]. The thickness of the electropolymerized films ranged from 900 to 1100 nm.

The gel electrolyte (GE) used in our photo-electrochemical (PEC) studies was synthesized following the procedure outlined in our previous work [16]. In the typical preparation, a solution containing potassium iodide (KI) at a concentration of 0.65 M and iodine (I_2) at 0.065 M was mixed with 10 mL of propylene carbonate (PC) and 8.5 g of polyethylene glycol (PEG) with a molecular weight of 20,000. This mixture was stirred continuously at 100˚C for approximately 12 hours under an inert gas atmosphere. Afterward, it was treated hydrothermally in a Teflon-lined autoclave at 180˚C for 14 hours.

2.3. Instrumentation

For the electrochemical preparation of the photoactive polymer, A typical three-electrode cell, with a platinum (Pt) wire serving as a counter electrode, Ag/AgCl as a reference electrode, and FTO with a surface area of 2.0 cm^2, was used as the working electrode. Photo-electrochemical (PEC) studies of the thin solid films were performed using the experimental setup as described in previous work [16]. Platinized FTO is used as both the reference and counter electrode due to its high conductivity in gel electrolytes and improved light transparency. A Solartron 2101A was used for electrochemical impedance spectroscopy (EIS) studies conducted over the frequency range 0.01 to 100 kHz. A BAS 100W electrochemical analyzer (Bioanalytical Co., IN) was used to perform electrochemical studies. Optical parameters were calculated based on the steady-state reflectance spectra, measured by a Shimadzu UV-2101PC spectrophotometer. Irradiation was performed using an Olympus BX-FL 300-watt xenon lamp solar simulator (Newport, NJ) with an IR filter. All measurements were performed at 298 K. All potentials were measured against pFTO (platinized FTO) (0.400 vs. Ag/AgCl).

2.4. Microscopy

The structure and autofluorescence of thin organic films were observed using brightfield and epifluorescence microscopy with an Olympus BX60 microscope (Olympus America, Inc., Melville, NY). The fluorescence ultraviolet filter produces an excitation band ranging from 330 to 385 nm with a barrier filter at 420 nm, and an irradiance of approximately 6.0 W/m2. Digital images were captured

with an Olympus DP70 Digital CCD Camera system and processed using IPLab Imaging Software (Scanalytics, Inc., Rockville, MD).

2.5. Computational Procedures

To elucidate the molecular origin of the observed trends in the photoactivity of PSNS, quantum chemical calculations were performed using ORCA 5.0.4 [17]. Geometry optimizations were carried out within the framework of density functional theory (DFT) employing the B3LYP in conjunction with the def2-TZVP basis set. Subsequently, electronic structure calculations were conducted at the B3LYP-D3/def2-SVP level of theory to determine the energies of the molecular orbitals, including the highest occupied molecular orbital (HOMO) and lowest unoccupied molecular orbital (LUMO), as well as the corresponding HOMO-LUMO energy gaps. The resulting molecular orbitals were analyzed and visualized using IboView [18]. All computational studies were performed on Quartz, Indiana University's high-performance, high-throughput computing cluster.

3. Results and Discussion

3.1. Absorption Spectra Studies

The absorption spectra of the assembly composed of FTO/PSNS have been collected and analyzed. For comparison, assemblies composed of poly-bithiophene (PBTh) were also studied to investigate the structural effects of replacing one sulfur (S) atom with a nitrogen (N) atom. **Figure 1** displays the obtained results. In **Figure 1(A)**, trace 1 shows a broader absorption with multiple peaks for PSNS, while **Figure 1(A)**, trace 2, shows a well-defined absorption peak for PBTh in the energy range between 2.3 and 3.1 eV. The appearance of multiple peaks reflects the presence of several oligomers with different HOMO/LUMO gaps [10]. Furthermore, **Figure 1(A)** indicates that the incorporation of the pyrrole ring results in a narrower HOMO-LUMO gap. This narrowing of the redshift allows the material to absorb light at longer wavelengths, shifting it towards the visible/NIR spectrum compared to unsubstituted bithiophene. This phenomenon explains why PSNS exhibits greater absorption than PBTh in the energy range of 1.5 to 2 eV.

Figure 1(B) presents a plot of the calculated refractive index (n) for the same polymers. Trace 1 in **Figure 1(B)** illustrates the change in n with the absorbed photon energy by PSNS, while trace 2 represents PBTh. The figure clearly shows that the refractive index for PBTh is greater than that of PSNS throughout the studied photon energy range. The higher the n of any material, the slower the light movement within the material. Slow light enhances the local optical density and intensity of light within the polymer, which directly increases the generation rate of photo-excited electrons and holes (polarons/bipolarons).

The Tauc plots shown in **Figure 2** were utilized to analyze the absorption data presented in **Figure 1**(A). The presence of several band gap values is indicated by the intercepts with the X-axis. These plots are evidence of the existence of direct band gaps due to the presence of oligomers.

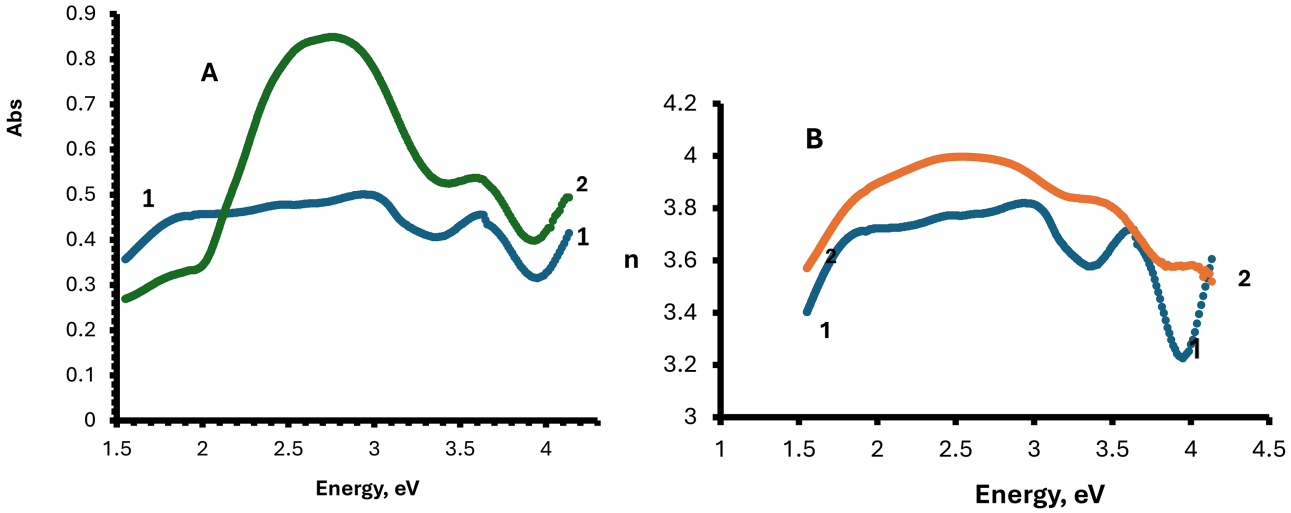

Figure 1. (A) Absorption spectra, (B) n vs photon energy. PSNS (trace 1) and PBTh (trace 2).

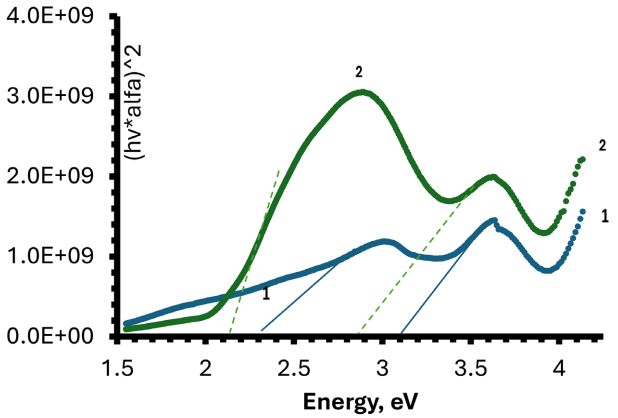

Figure 2. Tauc plot for PSNS (trace 1) and for PBTh (trace 2).

Figure 3 displays the relationship between the HOMO/LUMO energy gap and the reciprocal of the heterocyclic monomer unit numbers (N) in PSNS. The linear relationship shown in **Figure 3** also indicates that a polymer with at least 20 monomers would possess a bandgap of ≈ 2.0 eV. The multiple absorption peaks shown in **Figure 1** indicate the presence of several oligomers. The peaks with the highest band gaps correspond to trapped monomers, while those with lower band gaps correspond to entrapped dimers, trimers, and larger oligomers. This aligns with the structures optimized by density functional theory (DFT) shown in **Figure 3**. Similar DFT studies done on PBTh [10] show that PBTh possesses a band gap of 2.4. eV.

The higher optical conductivity (σ) of PBTh compared to PSNS in the 2.1 - 4.1 eV range (see **Figure 4**, Trace 1 vs. Trace 2) can be attributed to more effective charge delocalization in PBTh. The continuous conjugation along the polythiophene backbone in PBTh likely results in a higher density of free charge carriers. In contrast, the lower σ value for PSNS indicates that the addition of the pyrrole unit introduces some steric hindrance, disrupting the conjugation pathway. We believe this disruption occurs because the nitrogen atom (N) has higher electro-

negativity than the sulfur atom (S), which may increase the barrier to charge movement.

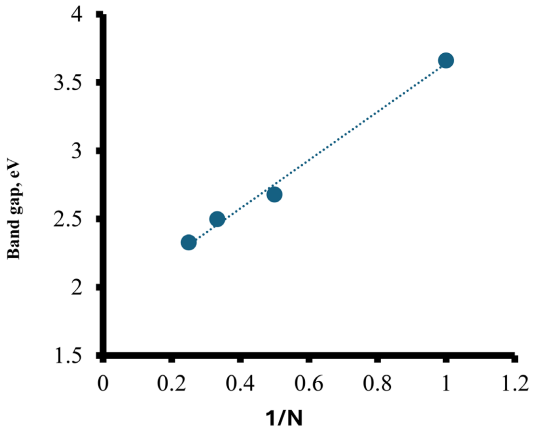

Figure 3. HOMO/LUMO gaps vs the reciprocal of SNS units.

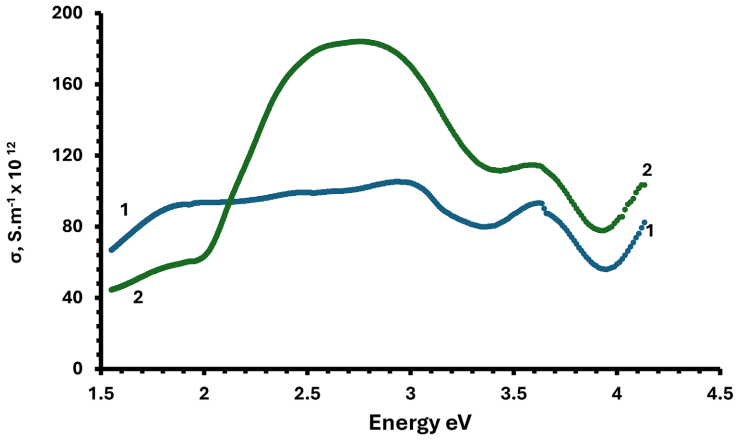

Figure 4. Optical conductivity of PSNS (trace 1) and of PBTh (trace 2).

3.2. Emission Spectra Studies on PSNS

Considering the average band gap of PSNS, which is approximately 2.3 eV as indicated by absorption spectra, Tauc plots, and DFT calculations, the excitation wavelength required to generate fluorescence should be shorter than about 540 nm. Therefore, using a white LED or UV for excitation can effectively produce fluorescence.

Figure 5 presents the emission spectrum of PSNS obtained after excitation with a white LED (wavelengths of 450 - 460 nm and 550 - 668 nm). The presence of a shoulder following the peak at 452 nm indicates fluorescence emission, which is denoted as the peak labeled "a". However, this fluorescence is completely overshadowed by the dominant blue peak at 452 nm. Inset 1 in Figure 5 shows the fluorescence emission of PSNS using UV excitation, while inset 2 displays a microscopic image of the electrodeposited PSNS film on FTO. Additionally, fluorescence emissions potentially generated between 500 and 700 nm are obscured by

the broad peak of the LED's phosphor emission.

In PSNS, some rotation restrictions may occur. This enhances fluorescence by increasing rigidity and reducing existing disorder. The thin solid film of PSNS exhibits structural rigidity and π-conjugated systems that limit motion. This leads to increasing the radiative decay (fluorescence) and thereby increases fluorescence intensity.

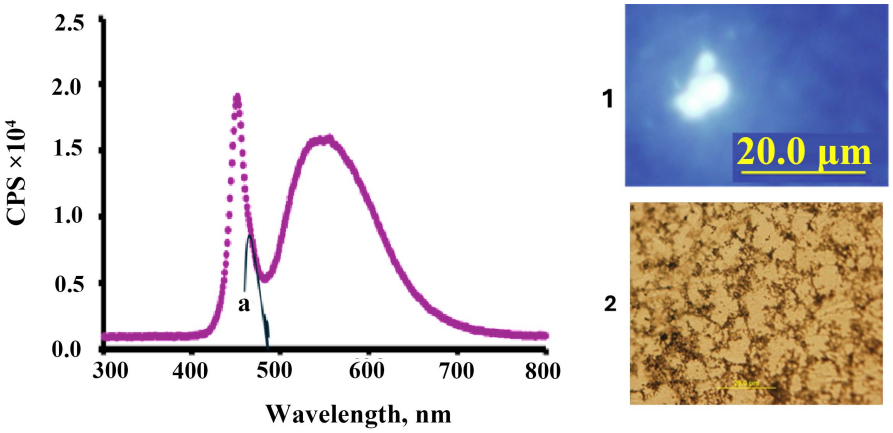

Figure 5. Fluorescence spectra of PSNS, inset 1- fluorescence image of PSNS using UV excitation, 2- microscopic image of the electrodeposited film of PSNS on FTO.

3.3. Photo-Electrochemical (PEC) Behavior

Polymer thin films were prepared by oxidative electropolymerization. This involved repetitively cycling the potential of a fluorine-doped tin oxide (FTO) substrate at a scan rate of 0.1 V/s between −1.0 V and 1.6 V versus Ag/AgCl. The electrolyte used was a 0.1 M solution of lithium perchlorate ($LiClO_4$) in acetonitrile, containing 10 mM of the monomer, and the process was carried out at room temperature in a cell described in the instrumentation section. The thickness of the film generated after 3 CV cycles ranged between 900 and 1100 nm.

In oxidative electropolymerization experiments, the reported oxidation potential for generating PSNS from its monomer was approximately 1.0 V vs. Ag/AgCl. This corresponds to an ionization potential (IP) of about 5.8 eV on the vacuum scale. In contrast, the reported values for PBTh were 1.2 V vs. Ag/AgCl for the oxidation potential and 6.0 eV for the ionization potential. These results indicate that the presence of a pyrrole ring lowers the oxidation potential compared to that of PBTh.

All photo-electrochemical studies performed in gel electrolyte took place in the electrochemical cell described in [16], where the modified FTO with either PSNS or PBTh as the working electrode, thermoplastic KI/I_3-gel acts as an electrolyte, and platinized FTO (Pt/FTO) acts as both counter and reference electrode.

PEC studies were performed in the dark and under illumination, with a scan rate of 0.10 $V{\cdot}s^{-1}$ between −1.5 and 2.0 V unless otherwise stated. The results are displayed in Figure 6 and Figure 7.

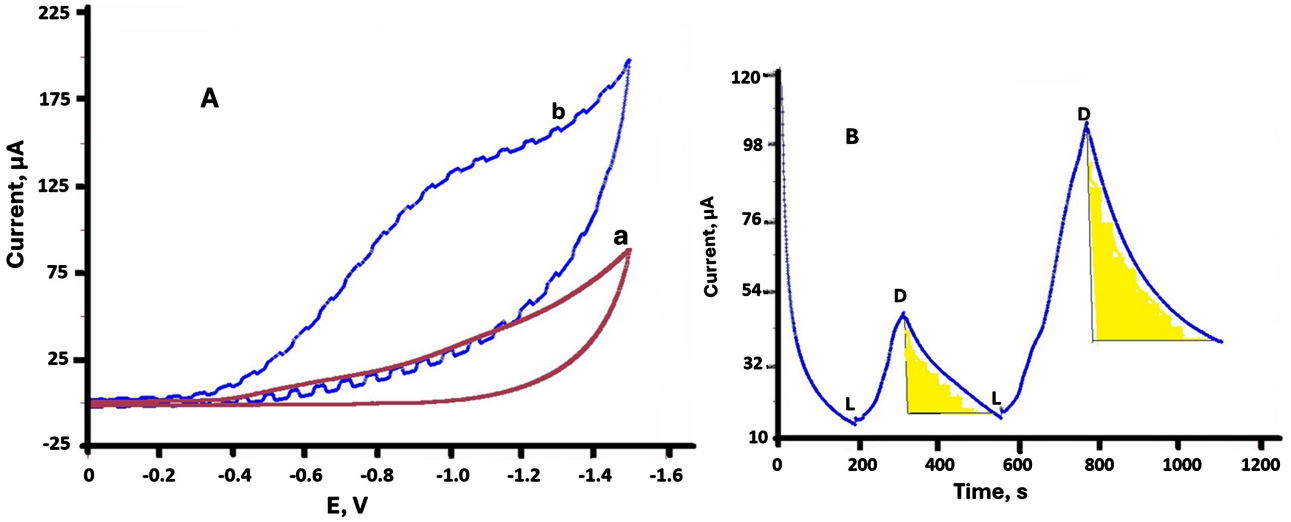

Figure 6. (A) I/µA and E/V at scan rate 0.1 V·s^{-1} for FTO/PSNS gel electrolyte, a) dark, b) illumination, and (B) chronoamperometric studies at −1.2 V vs. pFTO for FTO/PSNS. (D = Dark, L = under illumination). Shaded areas represent dark current.

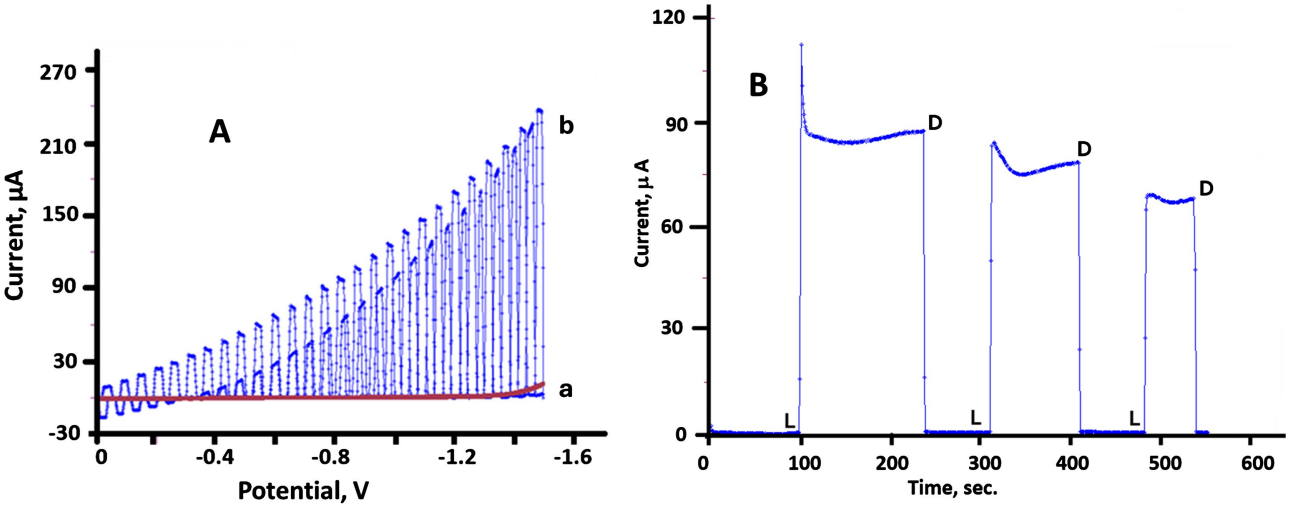

Figure 7. (A) I/µA and E/V at scan rate 0.1 V·s^{-1} for FTO/PBTh gel electrolyte, in a) dark, b) illumination, (B) chronoamperometric studies at −1.2 V vs. platinized FTO. (D = dark, L = under illumination).

Figure 6(A) shows that when FTO/PSNS is illuminated, there is an increase in the photocurrent (trace b) at approximately −0.3 V vs. pFTO. This value indicates the approximate position of the flat-band potential. Figure 6(B) presents the chronoamperometric studies conducted at a negative bias of −1.2 V vs. pFTO. This figure demonstrates the absence of hole accumulation, as evidenced by the lack of transient photocurrent overshoots upon illumination and the long discharge curves (current decay) when the light is turned off. Instead, a gradual but consistent increase in photocurrent was observed. Additionally, in the dark, there is no abrupt drop in current but rather a slow discharge, as illustrated by the shaded area in Figure 6(B). This phenomenon is called dark current [19] [20]. Dark current refers to an unwanted electric current that flows even in the absence of light. It is primarily caused by thermal effects, crystal defects, and leakage at the material's surface, which results in the

random generation and trapping of electrons and holes.

Figure 7(A) shows the electrochemical behavior of FTO/PBTh in a gel electrolyte. Under illumination, the photocurrent (trace b) increases at approximately 0.10 V vs. pFTO. This value indicates the approximate position of the Fermi level. Additionally, **Figure 7(B)** displays two important facts: 1) the presence of hole accumulations, and 2) the absence of dark current. Considering that hole accumulations indicate [19]-[21], the physical accumulation of holes distorts the local energy bands, resulting in a localized reduction of the energy barrier. This facilitates enhanced tunneling or injection of opposite charges, leading to an imbalance during hole and electron recombination due to the slow motion of holes.

Sulfur is less electronegative and more polarizable, which facilitates stronger, more delocalized intermolecular π-stacking and stabilizes the positive charge (hole) more effectively. The larger 3p orbitals of sulfur should enhance orbital overlaps between adjacent polymer chains, reducing the bandgap and improving hole generation.

Comparing the PEC behavior of PBTh and that of PSNS, we can see that the presence of the Pyrrole ring with the thiophene ring as part of the monomer causes a very noticeable change in PEC behavior of the resulting polymer. The polymer that consists of an S-based heterocyclic monomer generates a better organic photoactive polymer than the mixed N, S-based monomer. In light of these results, PBTh can be a good candidate for OLEDs (Organic Light-Emitting Diodes), organic solar cells, and flexible, printable electronics, while PSNS can be used in organic electrochemical transistors (OECTs).

3.4. Electrochemical Impedance Spectroscopy (EIS)

Impedance spectra of the studied assemblies were measured in the range 10^5 - 10^{-1} Hz. Impedance complexes (Nyquist plot), generated from these assemblies on FTO substrate in the dark and under illumination, are displayed in **Figure 8** and **Figure 9**. **Figure 8** shows that, regardless of the applied potential, the FTO/PSNS/gel electrolyte assembly exhibits kinetic behavior at high frequencies and diffusive behavior at lower frequencies. **Figure 8** also illustrates that under a negative potential of −1.0 V (**Figure 8(A)**) or at a positive bias potential of 1.0 V (**Figure 8(B)**), there is an increase in the imaginary component of the impedance across all study frequencies. An increase in imaginary impedance when a photoactive polymer is illuminated in a gel electrolyte can be driven by light-induced charge accumulation and changes in interfacial capacitance at the polymer-electrolyte boundary [22]. In this context, an increase indicates that the imaginary impedance becomes more negative (*i.e.*, of greater magnitude) within specific frequency ranges, which directly suggests enhanced energy storage (capacitance) at the interface. **Figure 8(C)**, however, indicates that at 0 V, there is no tangible effect of the illumination.

It is crucial to emphasize that there is no interception of the semicircle at high frequency (**Figure 8(C)** Insite). To achieve zero imaginary impedance at high frequency, only resistance should be present in the measured impedance. In the Nyquist plot, each point represents a complex contribution from the true

resistance (R), inductance (L), and capacitance (C). While L and C vary with frequency, R remains constant regardless of frequency [23]. The lack of a semicircle intercept at high frequency under the applied potential of ca. −1.0 V can be attributed to the strong inductive effect. This accounts for the high imaginary value at high frequency. Figure 8 and Figure 9 show that PBTh EIS studies reveal that PSNS exhibits lower real impedance than PBTh. This can be correlated to several factors such as porosity, doping, and the morphology of each polymer.

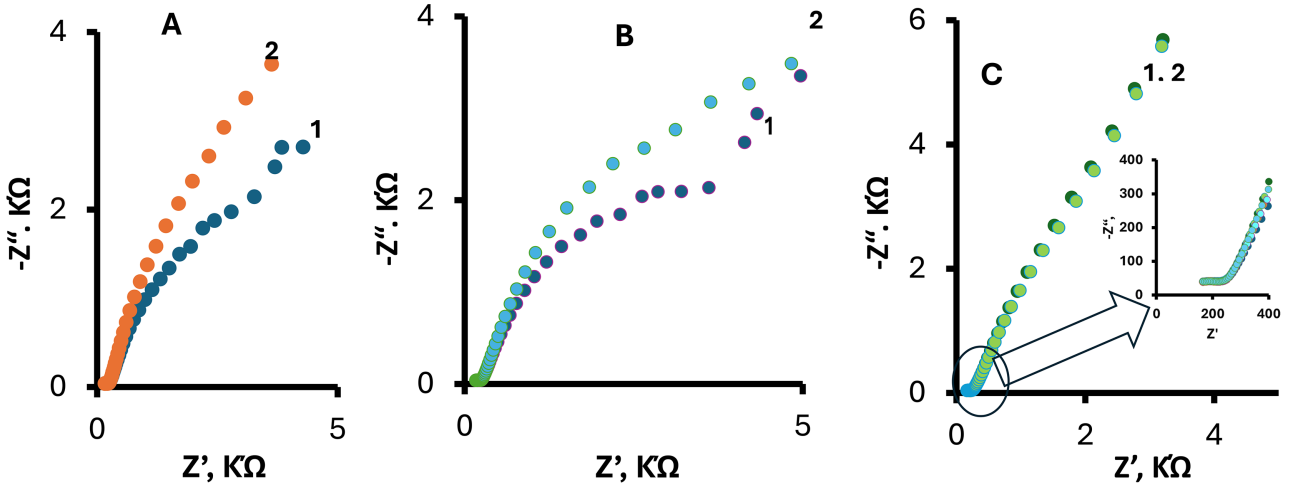

Figure 8. Nyquist plot of PSNS at (A) −1.0 V, (B) 1.0 V, and C) 0.0 V vs reference pFTO: 1 = dark, 2 = illumination. The inset is an expanded view.

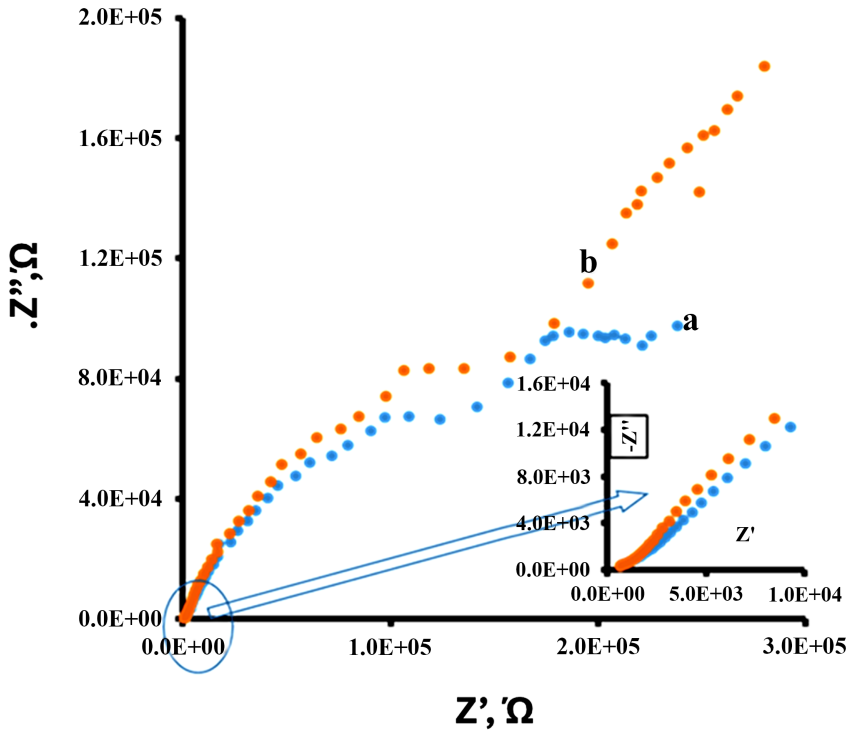

Figure 9. Nyquist plot of PBTh at −1.0 V vs reference pFTO, (a) Dark, (b) Illumination. The inset is an expanded view.

Figure 8 and Figure 9 also show both kinetic and diffusive control across the frequency range studied. The shape of an uncentered semicircle at high frequencies and the existence of Warburg impedance were attributed to the film porosity [23] [24]. Furthermore, Poly PBTh shows a higher real impedance than PSNS in gel electrolytes due to lower charge carrier mobility, denser film morphology, and reduced active sites for ion insertion [25].

4. Conclusion

The research results from spectroscopic and electrochemical techniques presented in this article demonstrate that adding a pyrrole ring to pure thiophene-based monomers significantly altered the PEC behavior, as evidenced by the comparison between the PEC results of PSNS and PBTh. The noticeable differences in the photo-electrochemical (PEC) behaviors of the two polymers support our prediction. We found that incorporating the pyrrole ring into a pure thiophene monomer yields a polymer whose PEC shows no evidence of hole accumulation. Instead, it illustrates the phenomenon of dark current, which is caused by random electron-hole pair production within the depletion layers at the interface. In contrast to this observed behavior, the PEC behavior of PBTh was that of an excellent hole accumulator, with a minimum cathodic discharge current. The minor differences in the HOMO/LUMO levels between PSNS and PBTh (due to changes in oxidation potential) and the properties that stem from these differences may not be the primary reason for the observed variations in their electrochemical behavior. It is assumed that the presence of pyrrole affects the polymer's dipole moments and morphology. These are the possible key properties that influence how charge carriers align and move across the boundary.

Acknowledgements

The authors would like to express their gratitude for the support received from the academic affairs office at Indiana University Kokomo.

Author Contributions

1) Kasem K. Kasem: Principal investigator, Electrochemical, Spectroscopic, EIS; 2) Christian Chauret: Fluorescence microscopy; 3) Hisako Masuda: DFT calculation and analysis; 4) O'Marrah Cullen Reily: Electrochemical/Spectroscopic/EIS; 5) Hermansen Hannah: Electrochemical/Spectroscopic/EIS.

Conflicts of Interest

The authors state that there are no conflicts of interest related to the publication of this paper.

References

[1] Wang, H. and Yan, D. (2010) Organic Heterostructures in Organic Field-Effect Transistors. *NPG Asia Materials*, **2**, 69-78. https://doi.org/10.1038/asiamat.2010.44

[2] He, Q., Liu, Y., Tan, C., Zhai, W., Nam, G. and Zhang, H. (2019) Quest for P-Type Two-Dimensional Semiconductors. *ACS Nano*, **13**, 12294-12300. https://doi.org/10.1021/acsnano.9b07618

[3] Xie, M., Pang, H., Wang, J., Cui, Z., Ding, H., Zheng, R., *et al.* (2024) Charge Balance in OLEDs: Optimization of Hole Injection Layer Using Novel P-Dopants. *Journal of the Society for Information Display*, **32**, 59-69. https://doi.org/10.1002/jsid.1271

[4] Ye, G., Li, S., Ding, R., Guo, R., Zhang, H., Liu, Z., *et al.* (2025) Unveiling the Interfacial Properties of Organic Single-Crystal Hole-Transporting Layers for High-Performance Light-Emitting Devices. *SmartMat*, **6**, e1329. https://doi.org/10.1002/smm2.1329

[5] Campbell, I.H., Kress, J.D., Martin, R.L., Smith, D.L., Barashkov, N.N. and Ferraris, J.P. (1997) Controlling Charge Injection in Organic Electronic Devices Using Self-Assembled Monolayers. *Applied Physics Letters*, **71**, 3528-3530. https://doi.org/10.1063/1.120381

[6] Boukhili, W., Chen, K., Wan, X., Tan, C.L., Sun, H., Yu, Z., *et al.* (2025) Organic-Inorganic Hybrid Injection Layers for Efficient Charge Injection in Organic Transistors. *Organic Electronics*, **147**, Article ID: 107332. https://doi.org/10.1016/j.orgel.2025.107332

[7] Higgins, S.J., Pounds, T.J. and Christensen, P.A. (2001) Syntheses and Electro(Co)Polymerization of Novel Thiophene- and 2,2':5',2"-Terthiophene-Functionalized Metal-Tetraazamacrocycle Complexes, and Electrochemical and Spectroelectrochemical Characterization of the Resulting Polythiophenes. *Journal of Materials Chemistry*, **11**, 2253-2261. https://doi.org/10.1039/b103284b

[8] Roncali, J. (1992) Conjugated Poly(Thiophenes): Synthesis, Functionalization, and Applications. *Chemical Reviews*, **92**, 711-738. https://doi.org/10.1021/cr00012a009

[9] McLeod, G.G., Mahboubian-Jones, M.G.B., Pethrick, R.A., Watson, S.D., Truong, N.D., Galin, J.C., *et al.* (1986) Synthesis, Electrochemical Polymerization and Properties of Poly(2,5-Di-(-2-Thienyl)-Pyrrole). *Polymer*, **27**, 455-458. https://doi.org/10.1016/0032-3861(86)90165-5

[10] Kasem, K.K., Pu, J. and Cox, L. (2023) Photoactivities of Thiophene Monomer/Polymer Transition in Gel-Based Photo-electrochemical Assembly: A Theoretical/Experimental Approach. *International Journal of Electrochemical Science*, **18**, Article ID: 100077. https://doi.org/10.1016/j.ijoes.2023.100077

[11] Kasem, K.K., Osman, S.H., Jarrett, J. and Shultz, M. (2021) Electrochemical Optical, and Impedance Studies on Photoactive Assembles Consists of Mixed TiO_2-CdS Particles Occluded in Poly 2, 2' Bithiophene in Orthoorthophosphate and Citrate Electrolytes. Part II. *International Journal of Electrochemical Science*, **16**, Article ID: 150675. https://doi.org/10.20964/2021.01.17

[12] Waltman, R.J. and Bargon, J. (1986) Electrically Conducting Polymers: A Review of the Electropolymerization Reaction, of the Effects of Chemical Structure on Polymer Film Properties, and of Applications towards Technology. *Canadian Journal of Chemistry*, **64**, 76-95. https://doi.org/10.1139/v86-015

[13] Guernion, N.J.L. and Hayes, W. (2004) 3- and 3,4-Substituted Pyrroles and Thiophenes and Their Corresponding Polymers—A Review. *Current Organic Chemistry*, **8**, 637-651. https://doi.org/10.2174/1385272043370771

[14] İçli, M., Cihaner, A. and Önal, A.M. (2007) Anodic Polymerization of 2,5-Di-(2-Thienyl)-Furan in Ethanol. *Electrochimica Acta*, **52**, 8039-8043. https://doi.org/10.1016/j.electacta.2007.06.076

[15] Kasem, K., Masuda, H. and Mendez Rodriguez, A. (2024) Tracking the Photoactivity

at the Interface of Sic/Poly 2(2-Thienyl) Furan Thin Solid Film in Polymer Gel Electrolytes. *Journal of Electrochemical Science and Engineering*, **14**, 671-684. https://doi.org/10.5599/jese.2401

[16] Kasem, K.K. (2021) Long-Term Activity of Thermoplastic Gel Electrolyte in a Photo-Electrochemical Assembly Involving Poly Bithiophene (PBTh) as Photoactive Working Electrode. *Journal of Materials Science and Chemical Engineering*, **9**, 1-11. https://doi.org/10.4236/msce.2021.96001

[17] Neese, F. (2022) Software Update: The Orca Program System—Version 5.0. *WIREs Computational Molecular Science*, **12**, e1606. https://doi.org/10.1002/wcms.1606

[18] Knizia, G. (2013) Intrinsic Atomic Orbitals: An Unbiased Bridge between Quantum Theory and Chemical Concepts. *Journal of Chemical Theory and Computation*, **9**, 4834-4843. https://doi.org/10.1021/ct400687b

[19] Labanti, C., Wu, J., Shin, J., Limbu, S., Yun, S., Fang, F., *et al*. (2022) Light-Intensity-Dependent Photoresponse Time of Organic Photodetectors and Its Molecular Origin. *Nature Communications*, **13**, Article No. 2745. https://doi.org/10.1038/s41467-022-31367-4

[20] McNeill, C.R., Hwang, I. and Greenham, N.C. (2009) Photocurrent Transients in All-Polymer Solar Cells: Trapping and Detrapping Effects. *Journal of Applied Physics*, **106**, Article ID: 024507. https://doi.org/10.1063/1.3177337

[21] Spadavecchia, F., Ardizzone, S., Cappelletti, G., Falciola, L., Ceotto, M. and Lotti, D. (2012) Investigation and Optimization of Photocurrent Transient Measurements on Nano-TiO_2. *Journal of Applied Electrochemistry*, **43**, 217-225. https://doi.org/10.1007/s10800-012-0485-2

[22] Saito, Y., Okano, M., Kubota, K., Sakai, T., Fujioka, J. and Kawakami, T. (2012) Evaluation of Interactive Effects on the Ionic Conduction Properties of Polymer Gel Electrolytes. *The Journal of Physical Chemistry B*, **116**, 10089-10097. https://doi.org/10.1021/jp3041814

[23] Chen, J., Unjaroen, D., Stepanovic, S., van Dam, A., Gruden, M. and Browne, W.R. (2018) Selective Photo-Induced Oxidation with O_2 of a Non-Heme Iron(III) Complex to a Bis(Imine-Pyridyl)Iron(II) Complex. *Inorganic Chemistry*, **57**, 4510-4515. https://doi.org/10.1021/acs.inorgchem.8b00187

[24] Bai, G., Liu, P., Guo, M., Yu, Y., Jiang, J., Hu, Y., *et al*. (2026) Bias-Switchable Broadband-Narrowband Organic Photodetectors Enabled by Vertical Phase Separation in Thick PM6: Y6 Bulk Heterojunctions. *ACS Applied Materials & Interfaces*, **18**, 12877-12888. https://doi.org/10.1021/acsami.5c23045

[25] Xie, X., Wang, Q., Mushtaq, F., Ao, K., Zhao, H. and Daoud, W.A. (2026) Adhesion Reinforcement of Electrode-Electrolyte Interface in Flexible Electrochemical Energy Storage Devices. *Nano-Micro Letters*, **18**, Article No. 255. https://doi.org/10.1007/s40820-026-02084-0